Isotope Effects in Dissociative Excitation of C_2H_2 and C_2D_2 by Collisions with Metastable Ne(3^P_0,2) Atoms

TSUJI, Masaharu
Institute for Materials Chemistry and Engineering, and Research and Education Center of Green Technology, Kyuhu University

KOMATSU, Takahiro
Department of Applied Science for Electronics and Materials, Interdisciplinary Graduate School of Engineering, Kyushu University : Graduate Student

UTO, Keiko
Institute for Materials Chemistry and Engineering, and Research and Education Center of Green Technology, Kyuhu University

HAYASHI, Jun-Ichiro
Institute for Materials Chemistry and Engineering, and Research and Education Center of Green Technology, Kyuhu University

他

https://doi.org/10.15017/4479588

出版情報：九州大学大学院総合理工学報告. 43 (1), pp.23-31, 2021-09. Interdisciplinary Graduate School of Engineering Sciences, Kyushu University
バージョン：
権利関係：

九州大学大学院総合理工学府報告
第 43 巻 第 1 号 22-31 頁 令和 3 年 9 月

Engineering Sciences Reports, Kyushu University
Vol. 43, No. 1, pp. 23-31, SEP, 2021

Isotope Effects in Dissociative Excitation of C_2H_2 and C_2D_2 by Collisions with Metastable Ne($^3P_{0,2}$) Atoms

Masaharu TSUJI*1,2† Tahahiro KOMATSU*3 Keiko UTO*1
Jun-Ichiro HAYASHI*1,2 and Takeshi TSUJI*4
†E-mail of corresponding author: tsuji@cm.kyushu-u.ac.jp

(Received May 24, 2021, accepted June 7, 2021)

Isotope effects in dissociative excitation of C_2H_2 and C_2D_2 by collisions with metastable Ne($^3P_{0,2}$) atoms have been studied in the Ne flowing afterglow. The CD($A^2\Delta$–$X^2\Pi_r$, $B^2\Sigma^-$ –$X^2\Pi_r$, and $C^2\Sigma^+$–$X^2\Pi_r$) and C_2($d^3\Pi_g$–$a^3\Pi_u$, $C^1\Pi_g$–$A^1\Pi_u$, $e^3\Pi_g$–$a^3\Pi_u$, and $D^1\Sigma_u^+$–$X^1\Sigma_g^+$) emission systems have been identified in the UV and visible region. The emission rate constants of CD(A,B,C) and C_2(d,C,e,D) were determined to be 1.7, 0.25, 0.014, and 5.4, 0.39, 0.12, 0.0046 × 10^{-13} cm^3 $molecule^{-1}$ s^{-1}, respectively. The isotopic ratios of $k_H(CH^*)/k_D(CD^*)$ and $k_H(C_2^*)/k_D(C_2^*)$ were determined to be 0.85 and 1.73, respectively. Although the reduction of emission rate constant of C_2^* from C_2D_2 is consistent with a simple dissociation model from the RRKM theory, the increase in the emission rate constant of CD* does not agree with it. The *inverse* isotope effect for CD* is explained by the fact that the formation of C_2^* and CH* or CD* occurs competitively, so that faster dissociation of C–H bonds suppresses the formation of CH*. Other possible mechanisms to explain the *inverse* isotope effect for CD* are discussed. The nascent vibrational and rotational distributions of CD(A:v'=0–2,B:v'=0) and C_2(d:v'=0–6, C:v'=0–3, e:v'=0–6, D:v'=0–2) were determined and compared with those obtained in the Ne($^3P_{0,2}$)/C_2H_2 reaction.

Key words: *Isotope effect, Dissociative excitation, Acetylene, Metastable Ne* atoms, Emission rate constant, Rovibrational distribution, Superexcited state, Reaction dynamics*

1. Introduction

In a preceding paper, we have studied the energy-transfer reaction of Ne($^3P_{0,2}$) with C_2H_2 in the Ne flowing afterglow.[1)] The CH($A^2\Delta$–$X^2\Pi_r$, $B^2\Sigma^-$ –$X^2\Pi_r$, and $C^2\Sigma^+$–$X^2\Pi_r$) and C_2($d^3\Pi_g$–$a^3\Pi_u$, $C^1\Pi_g$–$A^1\Pi_u$, $e^3\Pi_g$–$a^3\Pi_u$, and $D^1\Sigma_u^+$–$X^1\Sigma_g^+$) emission systems have been observed in the UV and visible region. Emission rate constants of CH(A,B,C) and C_2(d,C,e,D) were determined by using a reference reaction method. Rovibrational distributions of CH(A,B) and C_2(d,C,e,D) were determined from computer simulation of observed spectra. Significant vibrational excitation of C_2^* and rotational excitation of CH* and C_2^* were observed. When the observed vibrational and rotational distributions of CH(A,B) and C_2(d,C,e,D) were compared with statistical prior ones, large discrepancies were observed in most cases. These results suggested that CH* and C_2^* fragments are not formed through long-lived near-resonant $C_2H_2^{**}$ states, where excess energies are distributed in all internal degrees of freedom statistically. It was concluded that the most important factor, which dominates the reaction dynamics, is molecular structure of precursor state. CH(A,B) and C_2(d,C,e,D) are formed via *trans*-bent near-resonant Rydberg states converging to the first excited $\tilde{A}\ ^2A_g$ state of $C_2H_2^+$. Non-linear precursor superexcited states with enlarged C≡C bond and excited CCH bending vibration led to vibrationally excited C_2^* and rotationally excited CH* and C_2^* fragments.

In the present study, UV and visible emission spectra resulting from the Ne($^3P_2$: 16.62 eV, $^3P_0$:16.72 eV)/C_2D_2 reaction are measured in the Ne afterglow to obtain more information on the reaction dynamics from isotope effects. The emission rate constants of each emitting state and rovibrational distributions of excited states are determined and compared with those obtained from the Ne($^3P_{0,2}$)/C_2H_2 reaction.[1)]

*1 Institute for Materials Chemistry and Engineering, and Research and Education Center of Green Technology
*2 Department of Applied Science for Electronics and Materials
*3 Department of Applied Science for Electronics and Materials, Graduate Student
*4 Department of Materials Science, Shimane University

Isotope effects obtained are also compared with those reported in vacuum ultraviolet (VUV) photoexciation with similar excitation energies.[2,3]

2. Experimental

The FA apparatus equipped with UV and visible optical emission detection system was the same as that reported in the preceding paper.[1] C_2D_2 was synthesized by the reaction of CaC_2 with D_2O using a liquid nitrogen to suppress a rapid reaction.

$$CaC_2\ (g) + 2D_2O\ (l) \rightarrow Ca(OD)_2\ (s) + C_2D_2\ (g) \qquad (1)$$

Purity of CaC_2 and D_2O reagents were higher than 99.9%. The partial pressure of C_2D_2 in the reaction zone was 1–6 mTorr (1 Torr = 133.3 Pa).

3. Results

3.1 Emission spectra and dissociative excitation processes

Figure 1a shows a typical emission spectrum obtained from the Ne afterglow reaction of C_2D_2. The CD($A^2\Delta$–$X^2\Pi_r$ and $B^2\Sigma^-$–$X^2\Pi_r$) and C_2($d^3\Pi_g$–$a^3\Pi_u$ and $C^1\Pi_g$–$A^1\Pi_u$) emission systems are identified in the 330–570 nm region. In addition, CD($C^2\Sigma^+$–$X^2\Pi_r$) and C_2($e^3\Pi_g$–$a^3\Pi_u$ and $D^1\Sigma_u^+$–$X^1\Sigma_g^+$) emission systems are identified in the 314 nm and 210–300 nm region, respectively (not shown in Fig. 1a). For comparison, emission spectrum obtained from the Ne($^3P_{0,2}$)/C_2H_2 reaction is shown in Fig. 1b, where corresponding CH(A–X and B–X) and C_2(d–a and C–A) emission systems are observed. The most outstanding feature of the Ne($^3P_2$)/C_2D_2 spectrum is that the intensity ratio of C_2(d–a)/CD(A–X) becomes small in comparison with that of C_2(d–a)/CH(A–X) in the Ne($^3P_{0,2}$)/C_2H_2 reaction.

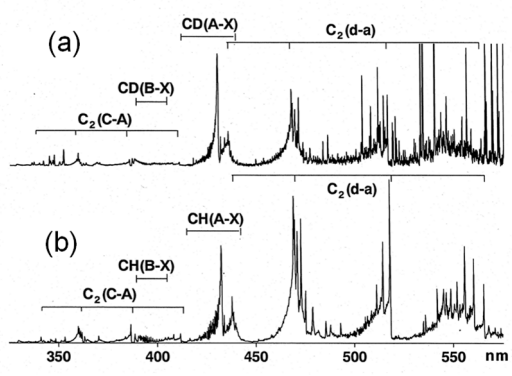

Fig. 1. Emission spectra obtained from the (a) Ne($^3P_{0,2}$)/C_2D_2 and (b) Ne($^3P_{0,2}$)/C_2H_2 reactions.

3.2 Emission rate constants of CD* and C_2*

CD(A,B) and C_2(d,C,e,D) are formed from the following energy-transfer reactions between Ne($^3P_2$) atoms and C_2D_2:

Ne($^3P_2$) + C_2D_2

$\rightarrow$ CD(A) + CD(X) + Ne + 3.61 eV, (2a)
$\rightarrow$ CD(B) + CD(X) + Ne + 3.29 eV, (2b)
$\rightarrow$ CD(C) + CD(X) + Ne + 2.55 eV, (2c)
$\rightarrow$ C_2(d) + 2D + Ne + 3.17 eV, (3a)
$\rightarrow$ C_2(d) + D_2 + Ne + 7.76 eV, (3b)
$\rightarrow$ C_2(C) + 2D + Ne + 1.40 eV, (3c)
$\rightarrow$ C_2(C) + D_2 + Ne + 6.00 eV, (3d)
$\rightarrow$ C_2(e) + 2D + Ne + 0.63 eV, (3e)
$\rightarrow$ C_2(e) + D_2 + Ne + 5.23 eV, (3f)
$\rightarrow$ C_2(D) + 2D + Ne + 0.41 eV, (3g)
$\rightarrow$ C_2(D) + D_2 + Ne + 5.01 eV. (3h)

The ΔH^o values were calculated using reported theremochemcial and spectroscopic data.[4,5] For the reactions with higher-energy Ne($^3P_0$) atoms, 0.10 eV higher excess energies are released in the above reactions. The excess energies released in the Ne($^3P_2$)/C_2D_2 reaction are smaller than those in the Ne($^3P_2$)/C_2H_2 reaction[1] by 0.05–0.17 eV.

Among above processes, highly exoergic reactions (3b), (3d), (3f), and (3h), in which D_2 molecules are formed, will be unfavorable, because large excess energies should be released as rovibrational energies and kinetic energies of products.

The emission rate constants for reactions (2)–(3) were determined by using the reference reaction method reported in our previous paper.[1] The Ne($^3P_{0,2}$)/NO reaction was used as a reference reaction.

$$Ne(^3P_{0,2}) + NO \rightarrow NO(A^2\Sigma^+) + Ne \qquad (4)$$
$$k_4 = 4.8 \times 10^{-11}\ cm^3\ molecule^{-1}\ s^{-1}$$

Emission rate constants of each species were estimated by comparing the integrated emission intensity of each band system with that of NO(A–X) in prepared mixtures of C_2D_2/NO. Results obtained are given in Table 1 along with our results for the Ne($^3P_{0,2}$)/C_2H_2 reaction.[1] If there is no nonradiative decay and pumping from the observation region, the emission rate constants equal the formation ones. Hereafter, k_H(X) and k_D(X) represent

Table 1. Emission rate constants of the excited fragments produced in the $Ne(^3P_{0,2})/C_2D_2$ and $Ne(^3P_{0,2})/C_2H_2$ reactions. ($\times 10^{-13}$ cm^3 molecule^{-1} s^{-1}).

$Ne(^3P_{0,2})$ /C_2D_2	k_D This work	$Ne(^3P_{0,2})$ /C_2H_2	k_H Ref. 1	k_H/k_D
CD(A)	1.7	CH(A)	1.5	0.88
CD(B)	0.25	CH(B)	0.22	0.88
CD(C)	0.014	CH(C)	0.0046	0.33
sum	2.0	sum	1.7	0.85
C_2(d)	5.4	C_2(d)	9.3	1.72
C_2(C)	0.39	C_2(C)	0.69	1.77
C_2(e)	0.12	C_2(e)	0.22	1.83
C_2(D)	0.0046	C_2(D)	0.0069	1.50
sum	5.9	sum	10.2	1.73
total	7.9	total	11.9	1.51

emission rate constants of excited species X produced from C_2H_2 and C_2D_2, respectively. The k_D (C_2*) and k_H (C_2*) values are larger than the k_D (CD*) and k_H (CH*) values by factors of 3.0 and 6.0, respectively. Here, C_2*, CD*, and CH* stand for C_2(d,C,e,D), CD(A,B,C), and CH(A,B,C), respectively. Results obtained imply that C_2* are more favorable excited products than CD* or CH* in the $Ne(^3P_{0,2})/C_2D_2$ and $Ne(^3P_{0,2})/C_2H_2$ reactions. Among CD(A,B,C) or CH(A,B,C) and C_2(d,C,e,D) products, the CD(A) or CH(A) and C_2(d) states are major product states. Actually, the k_D(CD(A)) and k_H(CH(A)) values occupy 85% and 88% of k_D(CD*) and k_H(CH*), whereas the k_D(C_2(d)) and k_H(C_2(d)) values occupy 92% and 91% of k_D(C_2*) and k_H(C_2*), respectively.

When deuterium isotope effects are examined, the following ratios are obtained for the total emission rate constants of CH* or CD* and C_2*.

$$k_H\,(CH^*) / k_D\,(CD^*) = 0.85 \quad (5a)$$
$$k_H\,(C_2^*) / k_D\,(C_2^*) = 1.73 \quad (5b)$$

It should be noted that the formation of CD(A,B,C) by C≡C scission is enhanced by the deuterium substitution, whereas the formation of C_2(d,C,e,D) by two C–D bond scissions are suppressed by the deuterium substitution. When the dependence of isotope ratio on the product state is examined, the isotope ratio of the major CH(A,B) states is the same (0.88), whereas that of the minor CH(C) state is very small (0.33). The isotope ratios for the major C_2(d,C,e) states are nearly the same (1.72–1.83), whereas that for the minor highest C_2(D) state (1.50) is smaller than the above major states. These results show that the dependence of isotope effects on the CH* and C_2* electronic states is small for the major CH(A,B) and C_2(d,C,e) states. Based on the above facts, we believe that similar reaction dynamics takes part in the formation of CH* or CD* and C_2* from dissociation of C_2H_2** and C_2D_2** superexcited states. Further detailed discussion about isotope effects will be given in the Discussion section.

3.3 Rovibrational distributions of CD(A,B) and C_2(d,C,e,D) in the $Ne(^3P_{0,2})/C_2D_2$ reaction

Rovibrational distributions of CD(A,B) and C_2(d,C,e,D) in the $Ne(^3P_{0,2})/C_2D_2$ reaction were determined by a computer simulation of emission spectra. The simulation procedure was the same as that used in the $Ne(^3P_{0,2})/C_2H_2$ reaction.[1)]

In Figs. 2–7 are shown the observed and best fit spectra of the CD(A–X, B–X) bands and C_2(d–a, C–A, e–a, and D–X) bands obtained assuming single Boltzmann rotational distributions for each v' level. Vibrational distributions and rotational temperatures thus obtained for CH(A,B) and C_2(d,C,e,D) are given in Tables 2 and 3, respectively. From the observed rovibrational distributions, we estimated the average vibrational and rotational energies of each CD* and C_2* state, denoted as $\langle E_v \rangle$ and $\langle E_r \rangle$, and the average yields of total available energy into these degrees of freedom, denoted as $\langle f_v \rangle$ and $\langle f_r \rangle$, respectively. Symbol $\langle f_t \rangle$ represents the average yield of total available energy into the relative translational energy. The $\langle E_v \rangle$, $\langle E_r \rangle$, $\langle f_v \rangle$, $\langle f_r \rangle$, and $\langle f_t \rangle$ values obtained for CD* and C_2* are summarized in Tables 4 and 5, respectively. For comparison, corresponding data of CH* and C_2* obtained in the $Ne(^3P_{0,2})/C_2H_2$ reaction[1)] are given.

On the basis of observed rovibrational distributions of CD* and C_2*, the following tendencies are found.

(A) Formation of CD*

(1) The vibrational population and rotational temperatures of CD(A:v'=0–2) are nearly the same as those of CH(A:v'=0–2) from C_2H_2[1)] except for a lower rotational temperature of 800 K for CD(A:v'=2). The

rotational temperatures of CD(B:v'=0) is higher than that of CH(B:v'=0) by 25%.[1)]

(2) The $<E_v>$ and $<f_v>$ values of CH(A) are larger than those of CD(A) by 25–30%. The $<E_r>$ and $<f_r>$ values of CH(A) are nearly the same as those of CD(A). The $<E_r>$ and $<f_r>$ values of CH(B) are smaller than those of CD(B) by 19–24%.

(3) The $<f_v>$ + $<f_r>$ value for CD(A) is 11.5%, whereas that for CD(B) is 8.2%. These results suggest that almost all (89% for CD(A) and 92% for CD(B)) of the total available energies are channeled into

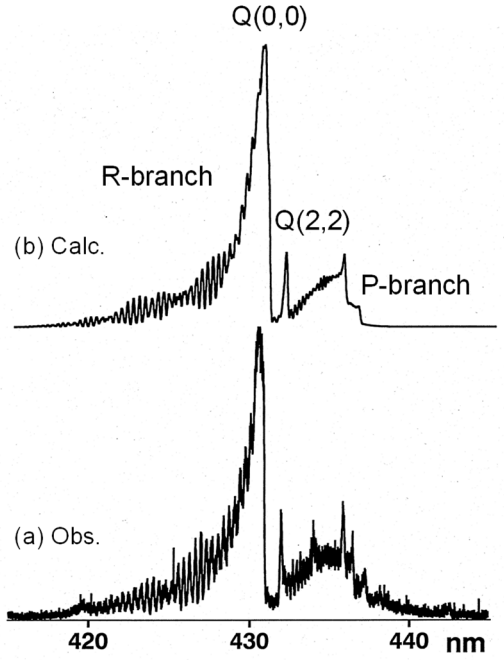

Fig. 2. (a) observed and (b) simulated emission spectra of CD($A^2\Delta$–$X^2\Pi_r$) band system obtained from the Ne($^3P_{0,2}$)/C_2D_2 reaction.

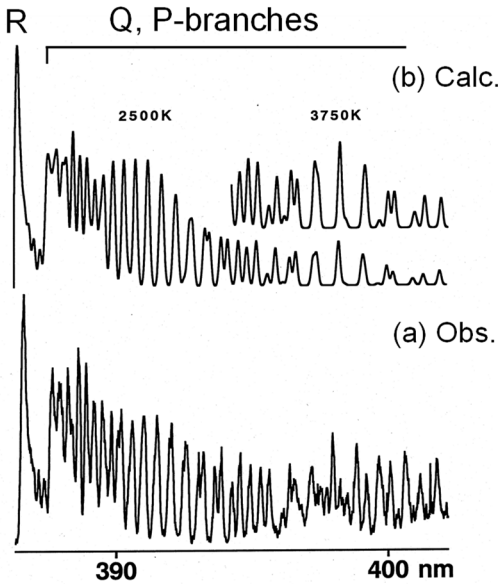

Fig. 3. (a) observed and (b) simulated emission spectra of (0,0) band of CD($B^2\Sigma^-$–$X^2\Pi_r$) band system obtained from the Ne($^3P_{0,2}$)/C_2D_2 reaction.

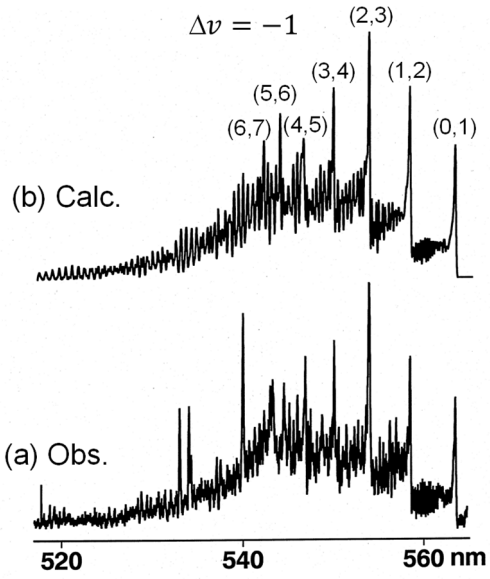

Fig. 4. (a) observed and (b) simulated emission spectra of C_2($d^3\Pi_g$–$a^3\Pi_u$) band system obtained from the Ne($^3P_{0,2}$)/C_2D_2 reaction.

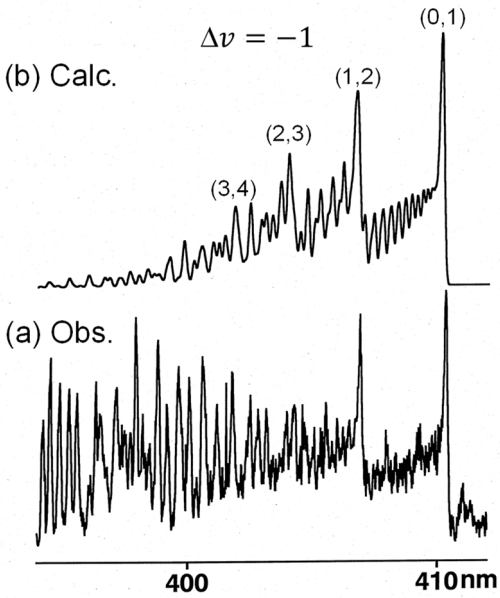

Fig. 5. (a) observed and (b) simulated emission spectra of C_2($C^1\Pi_g$–$A^1\Pi_u$) band system obtained from the Ne($^3P_{0,2}$)/C_2D_2

rovibrational energies of CD(X) and relative translational energy of CD(A or B) + CD(X) products, as in the case of CH* from C_2H_2.

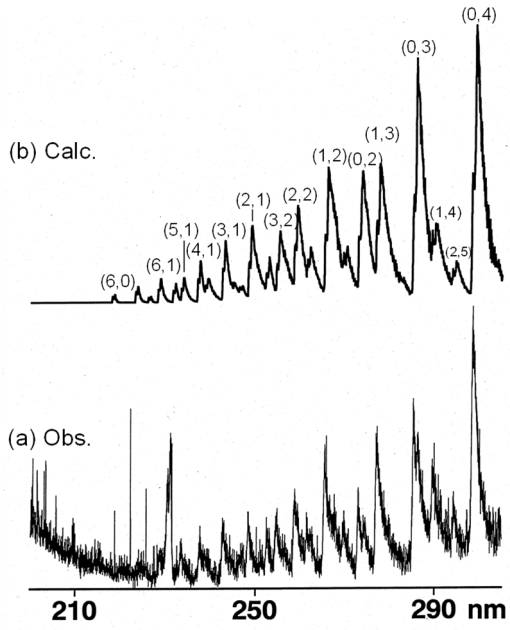

Fig. 6. (a) observed and (b) simulated emission spectra of $C_2(e^3\Pi_g–a^3\Pi_u)$ band system obtained from the $Ne(^3P_{0,2})/C_2D_2$ reaction.

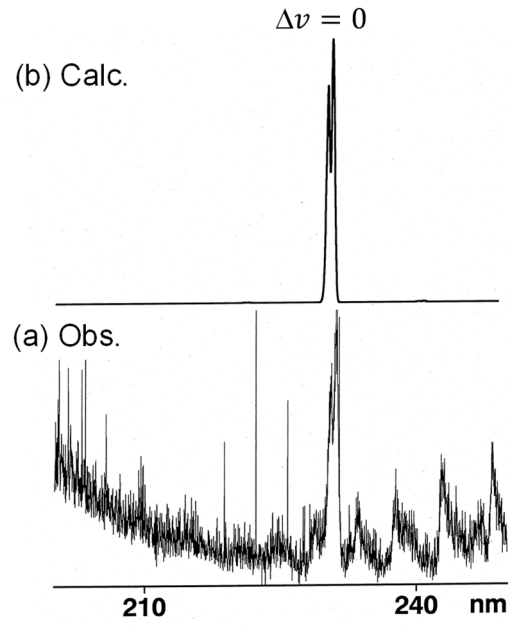

Fig. 7. (a) observed and (b) simulated emission spectra of $C_2(D^1\Sigma_u^+–X^1\Sigma_g^+)$ band system obtained from the $Ne(^3P_{0,2})/C_2D_2$ reaction.

(B) Formation of C_2*

(1) The vibrational populations of C_2(d,C,e,D) from C_2D_2 are the same as those from C_2H_2.[1] The rotational temperatures of C_2(d: v'=0–6) from C_2D_2 are higher than those from C_2H_2 by 62–82%, whereas those of C_2(C: v'=0–2) are higher than those from C_2H_2 by 10–25%.[1] The rotational temperatures of C_2(e: v' =0–6) and C_2(D: v'=0–2) are the same as those from C_2H_2.[1]

(2) The $<E_v>$ value of the lowest C_2(d) state from C_2D_2 is highest (0.53 eV), whereas those of the higher C_2(C,e,D) states are small (0.12–0.24 eV). The $<E_r>$ value of the lowest C_2(d) state (0.33 eV) is also higher than the other C_2(C,e,D) states (0.063–0.15 eV).

(3) The $<f_v>$ values for C_2(d,C,e,D) + 2D from C_2D_2 are larger than the $<f_r>$ values by factors of 1.4–2.9. These results indicate that deposition of excess energy into vibration is more favorable than that into rotation for the formation of C_2* + 2D from C_2D_2, as in the case of C_2* + 2H from C_2H_2.[1]

(4) The $<f_v>$ + $<f_r>$ values for C_2(d,C,e,D) + 2D from C_2D_2 are 27, 28, 32, and 60%, respectively. The C_2H_2/C_2D_2 ratios of $<f_v>$ + $<f_r>$ values for C_2(d,C,e,D) are 0.77–0.90. These results suggest that more excess energies are deposited into vibrational and rotational energies of C_2* by deuterium substitution.

3.4 Statistical models

As typical examples for the formation of CD* and C_2*, the formation dynamics of major CD(A) and C_2(d) products from the $Ne(^3P_{0,2})/C_2D_2$ system is discussed assuming two-body and three-body dissociation

Table. 2. Rovibrational distributions of CD(A,B) produced from the $Ne(^3P_{0,2})/C_2D_2$ reaction. $N_{v'}$ and $P^o_{v'}$ represent observed and calculated prior vibrational distributions, respectively. $P^o_{v'}$ were calculated assuming two-body and three-body dissociation processes.

Emitting species		$N_{v'}$	$P^o_{v'}$ Two-body	$P^o_{v'}$ Three-body	T_r / K
CD(A)	v'=0	100	100	100	4200
	v'=1	45	77	70	3000
	v'=2	8	60	49	800
CD(B)	v'=0	100			3125

Table 3. The rovibrational distributions of C_2(d,C,e,D) produced from the Ne($^3P_{0,2}$)/C_2D_2 reaction.

	C_2(d)			C_2(C)			C_2(e)			C_2(D)		
v'	$N_{v'}$	$P^o_{v'}$	T_r/ K	$N_{v'}$	$P^o_{v'}$	T_r/ K	$N_{v'}$	$P^o_{v'}$	T_r/ K	$N_{v'}$	$P^o_{v'}$	T_r/ K
0	100	100	5200	100	100	2250	100	100	1000	83	100	800
1	95	81	4500	60	60	1650	60	51	1200	100	9	800
2	88	65	4100	50	33	1250	27	22	700	43	0	450
3	55	51	3500	40	15	1000	12	14	400			
4	63	40	2900				7	7	300			
5	58	30	2500				3	1	300			
6	50	23	2100				1	0	300			

Table 4. Average vibrational and rotational energies (eV) deposited into CD (A,B) or CH(A,B) and average fractions (%) of vibrational and rotational energies deposited into CD(A,B) or CH(A,B) in the Ne($^3P_2$)/C_2D_2 and Ne($^3P_2$)/C_2H_2 reactions.

		C_2D_2	C_2H_2	C_2H_2 /C_2D_2
		This work	Ref. 1	
CD(A) or CH(A)	$<E_v>$	0.10	0.13	1.30
	$<E_r>$	0.32	0.32	1.00
	$<f_v>$	2.77	3.46	1.25
	$<f_r>$	8.75	8.60	0.98
	$<f_v>+<f_r>$	11.52	12.06	1.05
CD(B) or CH(B)	$<E_v>$	0.0	0.0	
	$<E_r>$	0.27	0.22	0.81
	$<f_v>$	0.0	0.0	
	$<f_r>$	8.18	6.21	0.76
	$<f_v>+<f_r>$	8.18	6.21	0.76

Table 5. Average vibrational and rotational energies deposited into C_2(d,C,e,D) and average fractions of vibrational, rotational, and translational energies deposited into C_2(d,C,e,D) in the Ne($^3P_2$)/C_2D_2 and Ne($^3P_2$)/C_2H_2 reactions.

		C_2D_2	C_2H_2	C_2H_2 /C_2D_2
		This work	Ref. 1	
C_2(d)	$<E_v>$	0.53	0.53	1.00
	$<E_r>$	0.33	0.19	0.58
	$<f_v>$	16.63	16.01	0.96
	$<f_r>$	10.34	5.75	0.56
	$<f_v>+<f_r>$	26.97	21.76	0.81
	$<f_t>$	73.03	78.24	1.07
C_2(C)	$<E_v>$	0.24	0.24	1.00
	$<E_r>$	0.15	0.13	0.87
	$<f_v>$	17.44	16.63	0.95
	$<f_r>$	10.50	8.60	0.82
	$<f_v>+<f_r>$	27.94	25.23	0.90
	$<f_t>$	72.06	74.77	1.04
C_2(e)	$<E_v>$	0.12	0.12	1.00
	$<E_r>$	0.082	0.082	1.00
	$<f_v>$	18.62	15.59	0.84
	$<f_r>$	12.88	10.78	0.84
	$<f_v>+<f_r>$	31.50	26.37	0.84
	$<f_t>$	68.50	73.63	1.07
C_2(D)	$<E_v>$	0.18	0.18	1.00
	$<E_r>$	0.063	0.063	1.00
	$<f_v>$	44.76	34.38	0.77
	$<f_r>$	15.44	11.86	0.77
	$<f_v>+<f_r>$	60.20	46.24	0.77
	$<f_t>$	39.80	53.76	1.35

mechanisms. The same models have been applied to the formation of CH(A,B) and C_2(d,C,e,D) from the Ne($^3P_2$)/C_2H_2 reaction.[1)]

(a) Two-body dissociation process through resonant excitation transfer

$$Ne^* + C_2D_2 \rightarrow C_2D_2^{**} + Ne$$
$$C_2D_2^{**} \rightarrow CD(A) + CD(X) \quad (6)$$

(b) Three-body dissociation process through resonant excitation transfer

$$Ne^* + C_2D_2 \rightarrow NeC_2D_2^{**}$$
$$NeC_2D_2^{**} \rightarrow CD(A) + CD(X) + Ne \quad (7)$$

(c) Three-body dissociation process through resonant excitation transfer

$$Ne^* + C_2D_2 \rightarrow C_2D_2^{**} + Ne$$
$$C_2D_2^{**} \rightarrow C_2(d,C,e,D) + 2D \quad (8)$$

Statistical vibrational and rotational distributions are calculated for the above three processes using the same equations reported in the preceding paper.[1)] As typical examples, the prior vibrational distribution of CD(A: v'=0–2)

and rotational distributions of CD(A: v'=0) for processes (a) and (b) are calculated and compared with the observed ones in Table 2

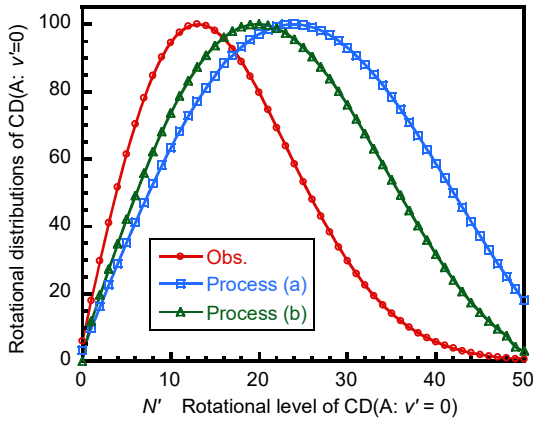

Fig. 8. Observed and two-body and three-body prior rotational distributions of CD(A: v'=0) in the Ne($^3P_{0,2}$)/C_2D_2 reaction.

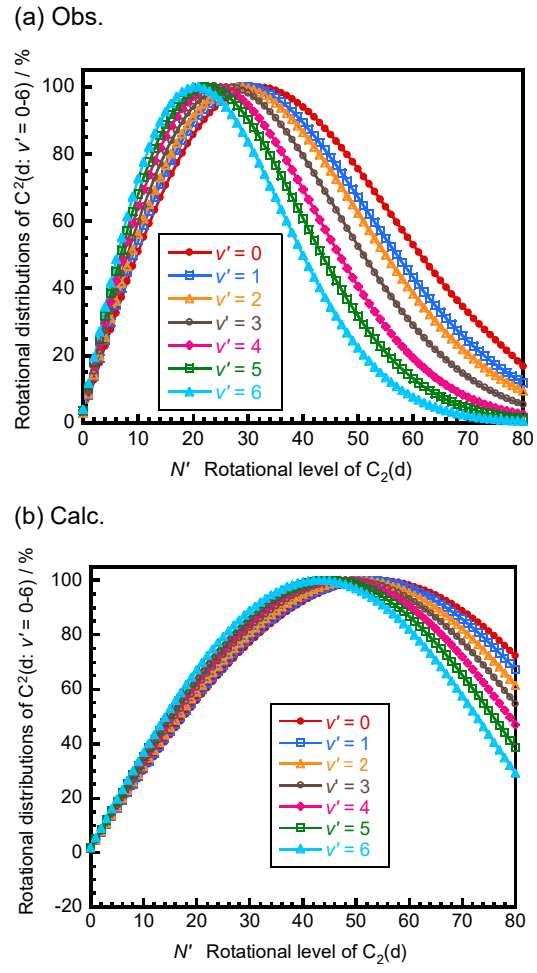

Fig. 9. (a) Observed and (b) calculated three-body prior rotational distributions of C_2(d: v'=0–6) in the Ne($^3P_{0,2}$)/C_2D_2 reaction.

and Fig. 8. The prior vibrational distribution of CD(A: v'=0–2) and rotational distributions of CD(A: v' =0) predict higher vibrational and rotational excitation than the observed ones for both two-body and three-body dissociation models, as observed in the case of CH(A) from C_2H_2.[1)]

The prior vibrational distributions of C_2(d,C,e,D) and rotational distributions of C_2(d: v'=0–6) calculated for three-body process (c) are compared with the observed ones in Table 3 and Figs. 9a and 9b. It should be noted that the observed vibrational distributions of C_2(d,C,D) are higher than prior ones, whereas a reasonable agreement between the observed and prior distributions is found for C_2(e). These results are opposite to those of CD(A), for which the observed vibrational distribution is lower than the prior one. On the other hand, the observed rotational distributions of C_2(d: v'=0–6) are lower than prior ones, as in the case of CD(A: v' =0). As shown above, similar discrepancies are observed between the observed vibrational and rotational distributions and statistical prior ones for the formation of CD* or CH* and C_2* from C_2D_2 and C_2H_2.

4. Discussion

4.1 Isotope effects in the Ne($^3P_{0,2}$)/C_2H_2 and Ne($^3P_{0,2}$)/C_2D_2 reactions

We found significant deuterium isotope effects on the formation rate constants of CH* (CD*) and C_2* from acetylene. Ibuki et al.[2,3)] measured isotope effects for the formation of CH* or CD* and C_2* under VUV photoexciation using NeI lamp and a synchrotron radiation. At photoexciation energy range of 11.62–11.72 eV, the following ratios have been determined for the emission cross sections, which are proportional to the emission rate constants.

$$k_H(CH^*)/k_D(CD^*) = 0.65–0.67 \quad (9a)$$
$$k_H(C_2^*)/k_D(C_2^*) = 1.52–1.53 \quad (9b)$$

It should be noted that similar *inverse* deuterium isotope effects are observed between CH* or CD* and C_2* in both Ne($^3P_{0,2}$) excitation and photoexcitation at similar excitation energies. However, the isotope effect on CH* obtained in the Ne($^3P_{0,2}$) excitation is smaller than that in VUV photoexcitation, whereas that on C_2* is larger than that in VUV photoexciation.

According to a simple RRKM theory,[3,6)]

kinetic hydrogen isotope effects for the formation of CH* or CD* and C_2 from C_2H_2 and C_2D_2 are expressed as follows.

$$k_H(CH^*)/k_D(CD^*) = (\mu_{C\text{-}CD}/\mu_{C\text{-}CH})^{1/2} = 1.02 \quad (10a)$$

$$k_H(C_2^*)/k_D(C_2^*) = (\mu_{C\text{-}D}/\mu_{C\text{-}H})^{1/2} \times (\mu_{C\text{-}D}/\mu_{C\text{-}H})^{1/2} = \mu_{C\text{-}D}/\mu_{C\text{-}H} = 1.86 \quad (10b)$$

Here, μ is the reduced mass. The observed isotope ratio for C_2^* in the Ne($^3P_{0,2}$) reaction, 1.73, is in reasonable agreement with the calculated value from Eq. 10b (1.86). It seems therefore reasonable to assume that the observed isotope effect on C_2^* in the Ne($^3P_{0,2}$) reaction originates from normal kinetic isotope effect between C–H and C–D bond scissions, which is independent on the spin-multiplicity of the precursor superexcited states.

The *inverse* isotope effect between CH and CD cannot be explained by the RRKM theory, which gives a larger value above 1. To explain the *inverse* isotope effects on C_2^* and CH* or CD*, Ibuki et al.[3] proposed two different mechanisms below 80 nm (>15.50 eV) and above 80 nm (<15.50 eV) region. The primarily important effect at the wavelength below 80 nm is the hydrogen isotope effect in the C–H and C–D bond dissociation which causes $k_H(C_2^*) > k_D(C_2^*)$. Because of the competition with these C–H and C–D bond dissociation channels, the processes leading to CH* and CD* radicals show an *inverse* isotope effect. They proposed four-membered cyclic isomer (Process A in Scheme 1), as one of the intermediate structures. The CC bond dissociation (A1) and the isomerization (A2) compete in the four-membered cyclic isomer. The probability of H atom migration in reaction (A2) should be higher than that of D atom due to the tunneling effect across the energy barrier. After the formation of $C{=}CH_2^{**}$ vinylidene, dissociation to C_2^* (B2) and the dark reactions (B3) and (B4) occur competitively, as shown in process B in Scheme 1. Dark dissociation processes (B3) and (B4) are more important for $C_2H_2^{**}$ because of faster formation rate of $C{=}CH_2^{**}$. The fact that the more $C{=}CH_2^{**}$ formation the weaker emission of CH* causes the *inverse* hydrogen isotope effect between the k_H(CH*) and k_D(CD*) values.

At the wavelengths longer than 80 nm, the dark processes (B3) and (B4), which are initiated by the isomerization via a *trans*-bent superexcited state to vinylidene, become important (Process B in Scheme 1). A tunneling

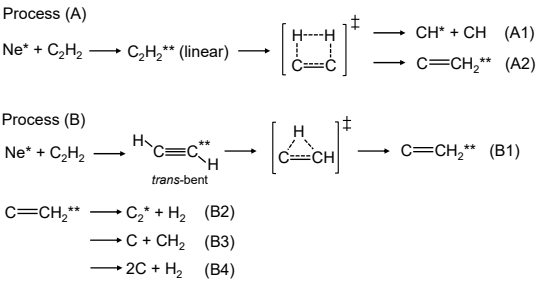

Scheme 1. Possible decomposition scheme of $C_2H_2^{**}$ in the Ne($^3P_{0,2}$)/C_2H_2 reaction.

effect on the H and D migration in the intermediates causes the *inverse* hydrogen isotope effect on the CH* and CD* emission intensities because the more $C{=}CH_2^{**}$ formation the weaker CH* emission.

In the Ne($^3P_{0,2}$) reaction, precursor $C_2H_2^{**}$ superexcited states of CH* and C_2^* are triplet Rydberg states, which are different from singlet Rydberg states formed under VUV photoexciation. However, it is reasonable to assume that similar mechanisms as proposed to explain isotope effects under VUV photoexciation are involved in the Ne($^3P_{0,2}$) reaction. In the case of photoexciation, C_2H_2 molecules are excited into a single resonant state with the same energy as that of incident photons. According to our systematic FA optical spectroscopic studies on energy-transfer reactions of rare gas metastable Ar($^3P_{0,2}$), Kr($^3P_{0,2}$), and Xe($^3P_{0,2}$) atoms with such small molecules as N_2 and CO, energy-transfer from Rg($^3P_{0,2}$) to molecules occurs near resonantly in most cases, where a few selective vibrational levels of triplet states are formed.[7-12] However, there was an exceptional case, where a wide vibrational distribution involving off-resonance states has been observed (e.g. Kr($^3P_{0,2}$) + N_2 → $N_2(B^3\Pi_g; v'=3-12)$ + Kr).[13] Therefore, we cannot exclude the possibility of the formation of several triplet $C_2H_2^{**}$ or $C_2D_2^{**}$ states with wide energy distributions in the Ne($^3P_{0,2}$) reaction. If products in wide energy distributions are formed, more than one mechanism will take part in the observed *inverse* isotope effect on CH* and CD*.

In our previous paper on the Ne($^3P_{0,2}$)/C_2H_2 reaction,[1] we concluded that CH(A,B) and C_2(d,C,e,D) are formed via *trans*-bent near-resonant $np\pi^* \leftarrow 3\sigma_g$ Rydberg states converging to the first excited $\tilde{A}\ ^2A_g$ state of $C_2H_2^+$. Non-linear precursor superexcited states with enlarged C≡C bond and excited CCH bending vibration led to vibrational excitation of C_2^* and rotational excitation of

CH* and C_2* radicals. It has been reported that the *trans*-bent $C_2H_2^+(\tilde{A}\ ^2A_g)$ ion generated at hν>16.351 eV (75.8 nm) is unimolecularly rearranged into the $\tilde{A}\ ^2A_1$ state of vinylidenic $C{=}CH_2^+$ ion.[14] The rearrangement to vinylidene, reaction (B1), is highly probable in the neutral superexcited acetylene, especially in its Rydberg states converging to *trans*-bent $C_2H_2^+(\tilde{A}\ ^2A_g)$ ion. Because of faster tunneling effect on the H and D migration in the intermediates, the more $C{=}CH_2$** formation causes the slower formation rate of CH*. Based on this fact, direct dissociation of *trans*-bent C_2H_2** and C_2D_2** into CH* and CD* completes with rearrangement to vinylidene form, which suppresses the CH* formation.

In the $Ne(^3P_{0,2})$ reaction, not only isomerization from *trans*-bent to three-membered cyclic transition state (B1) as described above, but also isomerization to non-linear four-membered cyclic isomer leading to the $C{=}CH_2$** formation (A2) may contribute to the *inverse* isotope effect between CH* and CD*. The formation of such non-linear intermediates with a loosen C≡C bond may also be one reason for the occurrence of high vibrational excitation of C_2* and high rotational excitation of CH* and C_2*. Further detailed experimental and theoretical studies on molecular structures and dissociation processes of high energy triplet Rydberg states are required to determine the relative importance of the above explanations for the *inverse* isotope effect for CH* (CD*) in the $Ne(^3P_{0,2})$ reaction.

5. Summary and Conclusion

Isotope effects for the formation of CH* or CD* and C_2* from the energy-transfer reactions of $Ne(^3P_{0,2})$ with C_2H_2 and C_2D_2 have been studied in the Ne flowing afterglow. The emission rate constants of CD(A,B,C) and C_2(d,C,e,D) in the $Ne(^3P_{0,2})/C_2D_2$ reaction were determined. The isotopic ratios of $k_H(CH^*)/k_D(CD^*)$ and $k_H(C_2^*)/k_D(C_2^*)$ were determined to be 0.85 and 1.73, respectively. The positive isotope effect for C_2* was consistent with that predicted from the RRKM theory because dissociation rate of C–H bond is faster than that of C–D bond. On the other hand, negative isotope effect for CH* (or CD*) does not agree with the prediction from the RRKM theory. It was explained by the fact that the formation of CH* or CD* competes with that of C_2* from dissociation of C–H bonds, so that faster dissociation of C–H bonds than C–D bonds suppresses the formation of CH*. Other possible mechanisms to explain the *inverse* isotope effect on CH* and CD* were proposed.

The nascent vibrational and rotational distributions of CD(A: v' =0–2,B: v' =0) and C_2(d: v'=0–6, C: v'=0–3, e: v'=0–6, D: v'=0–2) were determined. The vibrational distributions of CD(A,B) and C_2(d,C,e,D) from the $Ne(^3P_{0,2})/C_2D_2$ reaction were similar to those from the $Ne(^3P_{0,2})/C_2H_2$ reaction. The rotational temperatures of CD(A,B) were also similar to those of CH(A,B). The rotational temperatures of the lower C_2(d,C) states from the $Ne(^3P_{0,2})/C_2D_2$ reaction were higher than those from the $Ne(^3P_{0,2})/C_2H_2$ reaction. On the other hand, the rotational temperatures of the higher C_2(e,D) states from the $Ne(^3P_{0,2})/C_2D_2$ reaction were the same as those from the $Ne(^3P_{0,2})/C_2H_2$ reaction.

Acknowledgments

This work was supported by the Mitsubishi foundation (1996) and JSPS KAKENHI Grant number 09440201 (1997-2000).

References

1) M. Tsuji, T. Komatsu, K. Uto, J.-I. Hayashi, and T. Tsuji, *Engineering Sciences Reports, Kyushu University*, 43, 8 (2021).
2) T. Ibuki and Y. Horie, *Chem. Phys. Lett.*, 196, 541 (1992).
3) T. Ibuki, Y. Horie, A. Kamiuchi, Y. Morimoto, M. C. K. Tinone, K. Tanaka, and K. Honma, *J. Chem. Phys.*, 102, 5301 (1995).
4) *NIST Chemistry WebBook*, NIST Standard Reference Database, Number 69 (2018): http://webbook.nist.gov/chemistry.
5) K. P. Huber and G. Herzberg, "*Molecular Spectra and Molecular Structure, IV. Constants of Diatomic Molecules*", Van Nostrand Reinhold, New York (1979).
6) B. S. Rabinovitch and D. W. Setser, "*Advances in Photochemistry*, Vol. 3 ", Interscience, New York (1964) p. 1.
7) M. Tsuji, K. Yamaguchi, S. Yamaguchi, and Y. Nishimura, *Chem. Phys. Lett.*, 143, 482 (1988).
8) M. Tsuji, K. Yamaguchi, and Y. Nishimura, *Chem. Phys.*, 123, 151 (1988).
9) M. Tsuji, K. Yamaguchi, and Y. Nishimura, *Chem. Phys.*, 125, 337 (1988).
10) M. Tsuji, K. Yamaguchi, H. Obase, and Y. Nishimura, *Chem. Phys. Lett.*, 161, 41 (1989).
11) M. Tsuji, K. Yamaguchi, H. Kouno, and Y. Nishimura *Jpn. J. Appl. Phys.*, 30, 1281 (1991).
12) M. Tsuji, K. Yamaguchi, M. Kikukawa, H. Kouno, T. Funatsu, and Y. Nishimura, *Bull. Chem. Soc. Jpn.*, 65, 1713 (1992).
13) M. Tsuji, K. Yamaguchi, and Y. Nishimura *J. Chem. Phys.*, 89, 3391 (1988).
14) P. Rosmus, P. Botshwina, and J. P. Maier, *Chem. Phys. Lett.*, 84, 71 (1981).